Micro-refractive optical elements fabricated by multi-exposure lithography for laser speckle reduction

ZHAOMIN TONG,[1,2,*] FENG NIU,[1,2] ZEQUN JIAN,[1,2] CHANGYUAN SUN,[1,2] YIFEI MA,[1,2] MEI WANG,[1,2] SUOTANG JIA,[1,2] AND XUYUAN CHEN[1,2,3]

[1] *State Key Laboratory of Quantum Optics and Quantum Optics Devices, Institute of Laser Spectroscopy, Shanxi University, Taiyuan, Shanxi 030006, China*
[2] *Collaborative Innovation Center of Extreme Optics, Shanxi University, Taiyuan, Shanxi 030006, China*
[3] *Department of Microsystems, University of South-Eastern Norway, Borre N-3184, Norway*
*zhaomin.tong@sxu.edu.cn

Abstract: Laser speckle reduction with a macro refractive optical element (mROE) is restricted by the limited entrance facet size of light pipe. Here, we have fabricated a micro-ROE (μROE) that incorporates three-dimensional micro-optical structures. The μROE with 2×2 duplicated multi-level cells is made of SU-8 photoresist with the help of multi-exposure lithography process. When the μROE works together with the mROE, objective speckle contrast is reduced to 0.2, where the light source is a low-coherence multimode laser diode. In principle, more speckle reduction can be obtained by fabricating μROEs with more cells and larger height differences among the cells.

1. Introduction

Compared with wide bandwidth illumination light sources, for example, lamps and light emitting diodes, lasers in projection displays can extend color gamut. Other distinguished features of lasers are that they can provide extremely bright images, and they have very long lifetime etc [1]. Though lasers have the aforementioned superiorities, their temporal and spatial coherences cause speckle which degrades the image quality [2]. Speckle reduction, as a necessary technology in laser displays, can be obtained by polarization diversity, angle diversity, changing diffusers, and vibrating screens etc. [3−13] The co-shared speckle reduction mechanism of these time-varying methods is by generating different speckle patterns and summing them together during the integration time of human eyes (~50 ms) [14], *i.e.*, temporal integration [2]. Actuators are required to introduce the temporal disturbances, which are bulky, energy-consumed, and noisy. It is therefore highly demanded for the development of passive speckle reduction technologies to avoid the use of actuators.

Passive speckle reduction can be achieved using binary phase codes, Hadamard matrix diffusers, and diffractive optical elements [15−17]. Though these diffractive optical devices can effectively reduce speckle, they increase optical system etendue due to light diffractions and may cause extra optical power loss. Passive speckle reduction can also be obtained by generating uncorrelated laser sub-beams with equivalent light intensity using multiple reflections [18,19]. Optical path differences among the laser sub-beams are larger than laser coherence length, and hence speckles are suppressed when the laser sub-beams are spatially homogenized. In order to make light intensities among the laser sub-beams equivalent to maximize speckle reduction efficiency, complicated optical coatings to realize partial reflection areas with different reflectivity are required in [18], and polarization rotators such as spatial light modulators are demanded in [19]. Recently, we have reported a simpler uncorrelated laser sub-beams realization approach by

introducing a macro-refractive optical element (mROE) [20]. The mROE was composed by two groups of glasses which were assembled along horizontal and vertical directions. For each piece of glass, its planar dimensions were 1 mm in width and 18 mm in length. Along the direction of light propagation, the glasses had different heights varying from 0.5 mm to 2.5 mm with the same increment of 0.5 mm and from 3 mm to 15 mm with the same increment of 3 mm for the horizontally and vertically aligned groups, respectively. We found that the mROE in together with a light pipe for spatial homogenization purpose could reduce speckle. The entrance facet of the light pipe, however, had fixed dimensions of 4 mm × 4 mm, which constrained the maximum number of uncorrelated laser sub-beams obtained by the mROE because the planar dimensions of the mROE cells were 1 mm × 1 mm. In order to increase the number of the uncorrelated laser sub-beams being achieved, the planar dimensions of the mROE cells should be decreased.

In this paper, we have fabricated a micro-ROE (μROE) to increase the number of uncorrelated laser sub-beams obtained by ROEs for laser speckle reduction. The μROE is consisted of three-dimensional (3D) micro-optical structures that are fabricated by multi-exposure lithography process with a feature dimension of hundreds of micrometres. Because of the height difference among the 3D micro-optical structures, the spatial coherence of the laser passing through the μROE is destroyed by destroying laser temporal coherence. The modulated laser sub-beams illuminate a diffuser where speckles form. The speckles are superposed spatially, resulting in an image with reduced speckle. We have studied the influence of laser sources with different temporal coherence property on speckle reduction efficiency by a reassembled mROE, by the μROE, and by the combination of the mROE and the μROE, where we have found that speckle can be reduced more efficiently when a low-coherence laser diode is used. Compared with other speckle reduction methods, the μROE has merits such as motionless, etendue preserved, and facile et al.

## 2.   Device fabrication and characterization

SU-8 is a high aspect ratio negative photoresist with high thermal and chemical stability and high optical transparency above 360 nm wavelength. SU-8 is best suited for permanent applications after exposing and curing [21]. Stacking multilayers of SU-8 layers can form complex 3D structures using multiple exposures coupled with a single development step, *i.e.*, multi-exposure lithography [22−24]. Figure 1 illustrates the adopted multi-exposure lithography process to fabricate the 3D micro-optical structures. Combinations of spin coating/soft bake/exposure/post exposure bake/planarization steps are implemented in a sequential manner whereby each subsequent SU-8 layer is coated on top of the previous exposed one. Finally, the three exposed SU-8 layers are developed simultaneously, followed by a hard bake step.
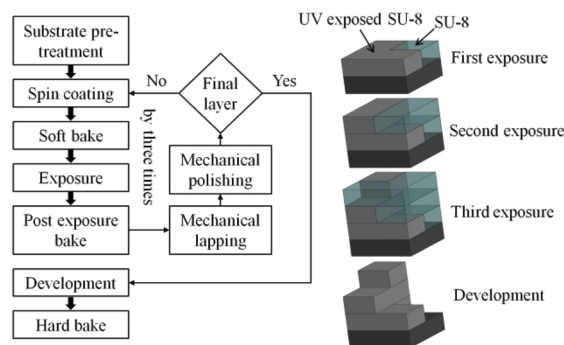
Fig. 1. Fabrication process of the SU-8 3D micro-optical structures by multi-exposure lithography.

As shown in Fig. 1, the first step is substrate pretreatment. A two-inch double side polished glass wafer (Borofloat 33 from Schott) is cleaned by acetone and isopropyl alcohol followed by a deionized water rinse. The glass wafer is baked for dehydration to ensure a good adhesion of the first SU-8 layer to the substrate. SU-8 (SU-8 2100 from Microchem) layers are spin-coated. The spin coating program for the first SU-8 layer includes a first coating with a spin speed of 500 rpm for 8 seconds at acceleration of 100 rpm·s^{-1} and a second coating with a spin speed of 1300 rpm for 30 seconds at acceleration of 300 rpm·s^{-1}; for the second and third SU-8 layers, similar spin parameters are used, but the spin speed for the second coating is increased to 1500 rpm. Thicknesses of the coated SU-8 layers are measured using a micrometer screw gauge, where the thickness of each SU-8 layer is about 230 µm. Soft bake is implemented with a contact hotplate, where the bake condition for the first coated SU-8 layer is 65°C for 7 minutes and 95°C for 45 minutes. In order to achieve the same bake effect for the upper SU-8 layers, longer soft bake time is used for the second and third SU-8 layers in comparison with the first one. The patterns on the photomasks are transferred to the SU-8 negative photoresists by a mask aligner (MA/BA6 from SUSS MicroTec), where an ultraviolet exposure dose of 9 mW·cm^{-2} for 62 seconds is used for all the three SU-8 layers. Reduced post exposure bake time is introduced due to the subsequent SU-8 layer soft bake time being generally longer than the prior layers soft bake time. In order to suppress the edge bead effect during the spin coating step and the surface curvature caused by the surface tension during the soft bake step, we have adopted a planarization step using chemical mechanical polishing including mechanical lapping and mechanical polishing [24]. The particle suspensions used for mechanically lapping and mechanically polishing are 6 µm and 0.1 µm in diameters, respectively. Planarization is stopped at a designed remaining layer thickness for each SU-8 layer. After the planarization step of the final SU-8 layer, a propylene-glycol-monomethyl-ether-acetate developer (from Microchem) is used to develop the exposed SU-8 multilayers with gentle agitation, where the development time is 40 minutes. The exposed SU-8 areas are left after development. A hard bake step is performed to increase the hardness and chemical resistance of the photoresist, where the hard bake temperature is 150 °C for 5 minutes.

By using the process flow presented in Fig. 1, we have fabricated a µROE with 2 × 2 duplicated 3D micro-optical structures. Considering that the minimum feasible dimension of the mROE cell in our lab is 0.4 mm, the planar dimensions of µROE cell are designed as $w_d = 200$ µm in width and $l_d = 200$ µm in length. Because SU-8 2100 has a recommended maximum film thickness at about 260 µm by single coat, the thickness of each SU-8 layer is designed as $t_d = 200$ µm, which is determined by thinning the 230 µm thick single spin-coated SU-8 layer using the aforementioned planarization step. Figure 2 shows the scanning electron microscope (SEM, SU8010 from Hitachi) and laser confocal microscope (LCM, OLS5000 from Olympus) images of the fabricated µROE with 3D micro-optical structures.
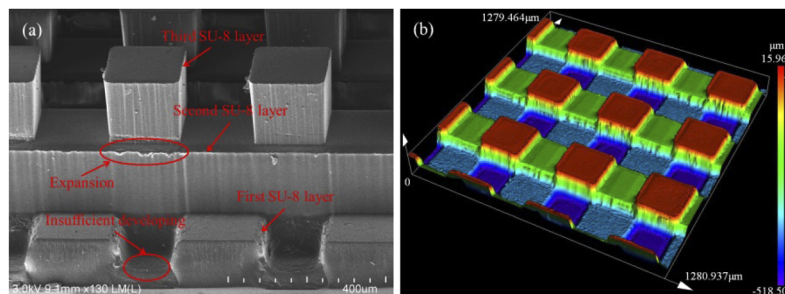

Fig. 2. Scanning electron microscope (a) and laser confocal microscope (b) images of the fabricated µROE with 3D micro-optical structures.

Both the SEM and LCM images in Fig. 2 confirm that the fabricated μROE have planar cell dimensions almost the same as the designed parameters. However, lateral expansion is observed for the underlying SU-8 layers, where Fig. 2(a) clearly shows the existence of the lateral expansion for the second SU-8 layer. Lateral expansion is mainly caused by the reabsorption of the base solvent into the underlying exposed SU-8 layers before it is fully crosslinked during the soft bake process [23]. The existence of lateral expansion affects the size of the μROE cell, which in turn causes inequivalent light intensities for the laser sub-beams and results in a higher reduced speckle contrast by the μROE. The LCM measurement in Fig. 2(b) indicates that the lateral expansion is not severe and is negligible. From Fig. 2(b), we can find that the average thicknesses of the SU-8 layers are different, which are $t_1 = 136$ μm, $t_2 = 192$ μm and $t_3 = 202$ μm for the first, second and third SU-8 layers, respectively. The significant thickness decrease of the first SU-8 layer is attributed to the insufficient developing; though the upper SU-8 layers have wider openings, the uncrosslinked photoresist in the first SU-8 layer cannot be fully dissolved by the solvent because of the openings are deep. The lateral expansion of the underlying SU-8 layers may also contribute to the thickness decrease for the underlying SU-8 layers, where the thickness of the second SU-8 layer t_2 is lower than the third SU-8 layer t_3.

3. Experiments and discussions

Figure 3 schematically shows the experimental setup for objective speckle measurement. A rotatable linear polarizer (53344 from Edmund Optics) is employed to adjust the light intensity of a linearly polarized and collimated laser beam. The laser beam is expanded by a beam expander, where a $\Phi_{iris} = 2$ mm in diameter iris is used to redefine the expanded laser beam size. An mROE composed by two orthogonal groups of glasses is placed after the iris, where the width and length of each piece of glass are 0.4 mm and 8 mm, respectively. The heights of the glasses arranged horizontally are 0.8 mm, 1.6 mm, 2.4 mm, and 3.2 mm, while these values are 4 mm, 8 mm, 12 mm, and 16 mm for the glasses positioned vertically. The two-inch μROE follows the mROE, and a sandblasted glass diffuser is used as light scattering rough object. Speckles formed on the diffuser are recorded by a charge-coupled device (CCD) camera (59356 from Edmund Optics). The CCD camera has a resolution of 2208×3000 and a pixel size of 3.5 μm $\times$ 3.5 μm. The exposure time of the CCD camera is a constant value of 50 ms, which is the same value as the integration time of human eyes [14]. In order to maintain the CCD camera working in its linear region, the linear polarizer is rotated correspondingly on different experimental conditions. The distance from the diffuser to the CCD camera is 500 mm. In case for subjective speckle measurement, a semitransparent object composed by another sandblasted glass diffuser and a plastic film with printed "SXU" logo is introduced after the first sandblasted glass diffuser (D in Fig. 3). In order to illuminate a large area on the semitransparent object, the distance between the first sandblasted glass diffuser and the semitransparent object is 50 mm. An imaging lens is mounted on the CCD camera, where the focal length and the F-number of the imaging lens are 35 mm and 22, respectively. The distance between the semitransparent object and the imaging lens is 200 mm.

A 0.8 mW HeNe laser (HNL008L from Thorlabs) and a multimode laser diode (LD, L520P50 from Thorlabs) with maximum output power of 50 mW are used as the laser light sources shown in Fig. 3. During the experiment, the driving current of the multimode LD is set at 120 mA, and the working temperature of the multimode LD is stabilized at 15 °C using a thermoelectric controller. The spectrums of the lasers are measured by a spectrometer (Aryelle Butterfly from LTB), where the results are shown in Fig. 4(a). From Fig. 4(a), we can find that the HeNe laser has a Gaussian spectral profile with the central wavelength of $\lambda_{HeNe} = 632.8$ nm and the spectral width (full width half maximum) of $\Delta\lambda_{HeNe} \approx 0.03$ nm; the multimode LD has a multiline spectrum profile with the central wavelength of $\lambda_{LD} = 525.2$ nm and the longitudinal mode spacing of $\Delta\lambda_{LD} \approx 0.08$ nm. Figures 4(b)–4(i) show objective speckles captured by the CCD camera
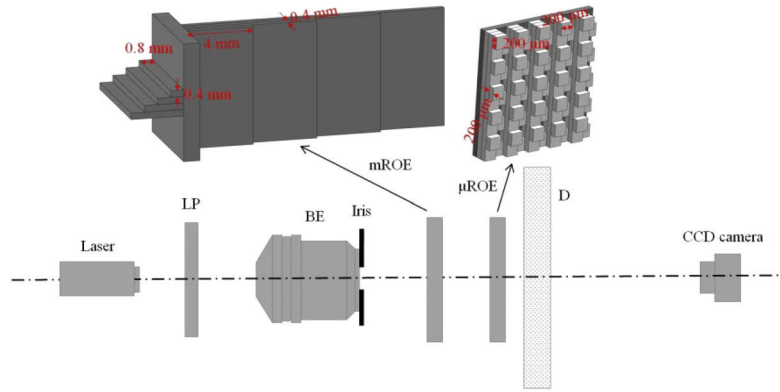
Fig. 3. Schematic of experimental setup for objective speckle measurement. LP: linear polarizer, BE: beam expander, mROE: macro-refractive optical element, µROE: micro-refractive optical element, D: diffuser, CCD: charge-coupled device.

under different experimental conditions. In case for the HeNe laser being used as the laser light source, we have not used ROEs in Fig. 4(b), and we have used mROE in Fig. 4(c), µROE in Fig. 4(d), and mROE and µROE in Fig. 4(e). Figures 4(f)–4(i) correspond to the conditions without ROEs, with mROE, with µROE, and with mROE and µROE, respectively. In Figs. 4(f)–4(i), the multimode LD is used as the laser light source. Figures 4(j)–4(m) show subjective speckles captured by the CCD camera under the corresponding experimental conditions to Figs. 4(f)–4(i).

Speckle contrasts C for the objective speckle images shown in Figs. 4(b)–4(i) are calculated by using $C = \sigma/<I>$, where σ and $<I>$ represent the standard deviation and mean value of speckle intensity, respectively. This equation is also introduced for calculating speckle contrasts for subjective speckle images shown in Figs. 4(j)–4(m), where we have selected the regions without "SXU" logo for calculation. For fully developed speckles, speckle contrast C equals to $1/2^{1/2} = 0.71$, where the degree of two is attributed to the depolarization of the rough object [2,3]. The speckle images shown in Figs. 4(b), 4(f), and 4(j) have speckle contrasts C higher than 0.71 because of diffuser partial depolarization. As shown in Fig. 4(a), the multimode LD has a more complicated spectrum distribution than the HeNe laser, thus, wavelength diversity results in lower speckle contrast of $C_{LD\_without\_o} = 0.79$ in Fig. 4(b) and $C_{LD\_without\_s} = 0.94$ in Fig. 4(j) for the multimode LD than $C_{HeNe\_without\_o} = 0.96$ in Fig. 4(f) for the HeNe laser.

In order to explain the speckle reduction mechanism by the ROEs, Fig. 5 schematically shows the mth and nth speckle patterns modulated by the corresponding ROE cells with heights of h_m and h_n, where speckles captured by the CCD camera are the spatial superposition of these speckle patterns.

For each ROE cell, it can generate a fully developed speckle pattern after passing through the diffuser with a speckle contrast of $C_0 = 1$ if there are no speckle reduction mechanisms being introduced. The sum of the N fully developed speckle patterns because of the N ROE cells has a reduced speckle contrast C_Σ given by [3]
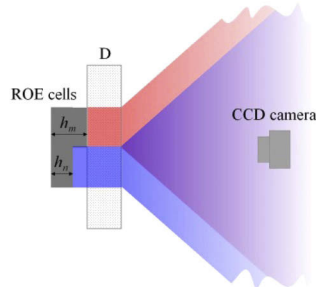
$$C_\Sigma = \frac{\sqrt{\sum_{m=1}^{N} \sum_{n=1}^{N} \sigma_m \sigma_n \rho_{m,n}}}{\sum_{n=1}^{N} \langle I_n \rangle} = \frac{\sqrt{\sum_{m=1}^{N} \sum_{n=1}^{N} \langle I_m \rangle \langle I_n \rangle \rho_{m,n}}}{\sum_{n=1}^{N} \langle I_n \rangle},\qquad(1)$$

where σ_m, σ_n, $<I_m>$ and $<I_n>$ represent the standard deviations and mean values of the mth and nth speckle intensities, respectively, $\rho_{m,n}$ is the correlation coefficient between the mth and nth speckle patterns that are generated by the corresponding mth and nth cells, and we have used the relationships of $\sigma_m = <I_m>$ and $\sigma_n = <I_n>$ for fully developed speckles [2]. Because the
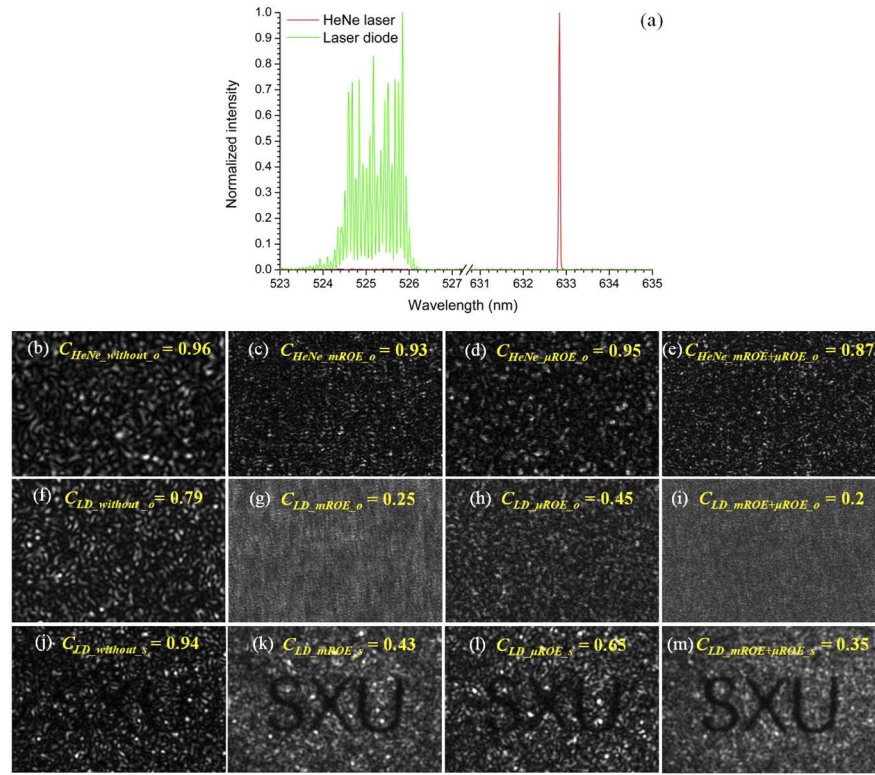
Fig. 4. Spectrums of the HeNe laser and the multimode laser diode (a). Objective speckles formed on the diffuser are captured by the CCD camera when the HeNe laser is used as the light source without ROEs (b), with mROE (c), with μROE (d), and with mROE and μROE (e). Objective speckles formed on the diffuser are captured by the CCD camera when the multimode laser diode is employed as the light source without ROEs (f), with mROE (g), with μROE (h), and with mROE and μROE (i). Subjective speckles when the multimode laser diode is employed as the light source without ROEs (j), with mROE (k), with μROE (l), and with mROE and μROE (m).

Fig. 5. Speckles capatured by the CCD camera are the spatial superpositon of the speckle patterns modulated by the ROE cells. D: diffuser.

expanded laser beam after transmitting through the iris has an almost uniform light intensity distribution across its cross section, the mean value of the speckle intensity $<I>$ formed by an individual ROE cell is proportional to the ROE cell area A; considering that the ROE cells have similar planar dimensions, *i.e.*, $A_m = A_n$ for the mth and nth ROE cells, we have $<I_m> =$ and $<I_n>$

$$C_\Sigma = \frac{\sqrt{\sum_{m=1}^{N} \sum_{n=1}^{N} \rho_{m,n}}}{N}. \tag{2}$$

From Eq. (2), it is reasonable that speckle can be reduced by the ROEs. This is because the value of $\rho_{m,n}$ fulfils the relationship of $\rho_{m,n} < 1$ due to the optical path difference between the mth and nth ROE cells having different heights of h_m and h_n for $m \neq n$. For the mROE schematically shown in Fig. 3, the laser beam with $\Phi_{iris} = 2$ mm in diameter beam width covers 5×5 mROE cells whose heights increases from $h_{mROE\_1} = 0$ mm to $h_{mROE\_25} = 19.2$ mm with an equivalent increment of 0.8 mm. As shown in Figs. 2 and 3, there are four cell heights for the μROE with 2×2 duplicated 3D micro-optical structures, which are $h_{\mu ROE\_1} = 0$ μm, $h_{\mu ROE\_2} = t_1 = 136$ μm, $h_{\mu ROE\_3} = t_1 + t_2 = 328$ μm and $h_{\mu ROE\_4} = t_1 + t_2 + t_3 = 530$ μm. Therefore, comparing with the μROE, the mROE can generate more laser sub-beams having larger optical path delays, *i.e.*, $N_{\mu ROE} < N_{mROE}$ and $\rho_{m,n\_\mu ROE} > \rho_{m,n\_mROE}$. The resulting effect is that speckle reduction achieved by the mROE is more efficient than by the μROE according to Eq. (2). Experimental results shown in Figs. 4(c) and 4(d), Figs. 4(g) and 4(h), and Figs. 4(k) and 4(l) are consistent with expectation. As we have mentioned above, the average thickness of each SU-8 layer is different, where $t_1 = 136$ μm is significantly lower than $t_2 = 192$ μm, $t_3 = 202$ μm and the expected layer thickness of $t_d = 200$ μm. The thinner SU-8 layer results in higher $\rho_{m,n\_\mu ROE}$, which causes a higher reduced speckle contrast than the expected value according to Eq. (2).

The fact that the multimode LD has more efficient speckle reduction than the HeNe laser after introducing the ROEs can be explained as follows. As shown in Fig. 4(a), it is obvious that the equivalent linewidth of the multimode LD $\Delta\nu_{c\_LD}$ is larger than that of the HeNe laser $\Delta\nu_{c\_HeNe}$, *i.e.*, $\Delta\nu_{c\_LD} > \Delta\nu_{c\_HeNe}$. Thus, the HeNe laser has shorter coherence time τ_c and longer coherence length l_c than the multimode LD because $\tau_c = 1/\Delta\nu_c$ and $l_c = c\tau_c$, where c is the speed of light [25]. When the laser beam transmits through the mROE or the μROE, the spatial coherence among the ROE cells are destroyed by destroying the temporal coherence of the lasers with the help of the optical path differences caused by the ROE cells with different heights. The spatial correlation coefficient between the mth and nth ROE cells with determinate height difference for the HeNe laser ρ_{m,n_HeNe} is always larger than that for the multimode LD ρ_{m,n_LD} because the relationship of $l_{c\_HeNe} > l_{c\_LD}$ holds. Therefore, from Eq. (2), we can also conclude that the reduced speckle contrast for the HeNe laser C_{Σ_HeNe} is always higher than that for the LD C_{Σ_LD} because the relationship of $\rho_{m,n\_HeNe} > \rho_{m,n\_LD}$ holds. This is confirmed by the experimental results shown in Figs. 4(c), 4(g), 4(d), and 4(h).

Another observation from Fig. 4 is that the combination of the mROE and the μROE shown in Figs. 4(e), 4(i), and 4(m) has higher speckle reduction efficiency than the mROE or the μROE alone. This is straightforward because $N_{mROE+\mu ROE} = 10 \times 10 = 100$ laser sub-beams are generated by the combination of the mROE and the μROE, while this numbers are $N_{mROE} = 5 \times 5 = 25$ and $N_{\mu ROE} = 2 \times 2 = 4$ by using the mROE and the μROE, respectively. According to Eq. (2), a larger number of N results in a lower reduced speckle contrast C_Σ.

Comparing the objective speckle images shown in Figs. 4(f)–4(i) and the corresponding subjective speckle images shown in Figs. 4(j)–4(m), we can find that the subjective speckle images always have higher speckle contrasts than the corresponding objective speckle images. This is because of the formation of compound speckle (or speckled speckle) [2]. In subjective speckle measurement, the first sandblasted glass diffuser (D in Fig. 3) causes the first speckle, and the semitransparent object creates another speckle. When the CCD camera captures the subjective speckle images formed on the semitransparent object, the two speckles (compound

speckle) increase the speckle contrast comparing with the condition when only a single speckle is formed (the condition for measuring objective speckles) [2].

The optical power loss after the introductions of the mROE and the μROE is about 20%. This is mainly caused by the reflections happened at the air/glass/air interfaces and the air/SU-8/air interfaces [25]. An additional antireflection coating process of the mROE and the μROE can suppress the optical power loss, but the cost of manufacturing ROEs will be increased.

4. Conclusions

In summary, we have fabricated a μROE which is consisted of 3D micro-optical structures by multi-exposure lithography for laser speckle reduction. We have experimentally investigated the speckle reduction ability of the μROE by using two kinds of laser sources: a high-coherence HeNe laser and a low-coherence multimode LD. The spatial coherence of the lasers is destroyed with the help of the μROE, thus, speckle is reduced when the speckle patterns generated by the μROE cells are spatially homogenized. We have studied the speckle reduction efficiency by the mROE, by the μROE, and by the combination of the mROE and the μROE. Because the number of the laser sub-beams and the optical path differences brought by the μROE are lower than those generated by the mROE, the μROE has lower speckle reduction efficiency than the mROE; while the μROE in together with the mROE is the best choice than by using the mROE or the μROE alone because of its highest speckle reduction efficiency.

The speckle contrasts obtained by the devices presented here is considerably higher than what has been reported for conventional speckle reduction methods, but optimization of the μROE, for example, by increasing the μROE cell number with larger cell height differences, is expected to improve device performance. Meanwhile, μROEs have advantages of being motionless, etendue preserved, and facile et al. In general, the technology concept by using multi-exposure lithography to fabricate μROEs is successfully demonstrated, and steps towards commercialization of the device are feasible.

Disclosures

The authors declare no conflicts of interest.

References

1. K. Chellappan, E. Erden, and H. Urey, "Laser-based displays: a review," Appl. Opt. **49**(25), F79–F98 (2010).
2. J. Goodman, *Speckle phenomena in optics: theory and applications* (Roberts and Company Publishers, 2006).
3. Z. Tong and X. Chen, "Speckle contrast for superposed speckle patterns created by rotating the orientation of laser polarization," J. Opt. Soc. Am. A **29**(10), 2074–2079 (2012).
4. G. Ouyang, M. Akram, K. Wang, Z. Tong, and X. Chen, "Laser speckle reduction based on angular diversity induced by Piezoelectric Benders," JEOS:RP **8**, 13025 (2013).
5. Z. Tong, X. Chen, M. Akram, and A. Aksnes, "Compound speckle characterization method and reduction by optical design," J. Disp. Technol. **8**(3), 132–137 (2012).
6. Z. Tong, W. Shen, S. Song, W. Cheng, Z. Cai, Y. Ma, L. Wei, W. Ma, L. Xiao, S. Jia, and X. Chen, "Combination of micro-scanning mirrors and multi-mode fibers for speckle reduction in high lumen laser projector applications," Opt. Express **25**(4), 3795–3804 (2017).
7. H. Chen, J. Pan, and Z. Yang, "Speckle reduction using deformable mirrors with diffusers in a laser pico-projector," Opt. Express **25**(15), 18140–18151 (2017).

8. S. Kubota and J. Goodman, "Very efficient speckle contrast reduction realized by moving diffuser device," Appl. Opt. **49**(23), 4385–4391 (2010).
9. Z. Tong and X. Chen, "Principle, design and fabrication of a passive binary micro-mirror array (BMMA) for speckle reduction in grating light valve (GLV) based laser projection displays," Sens. Actuators, A **210**, 209–216 (2014).
10. J. Lee, T. Kim, B. Yim, J. Bu, and Y. Kim, "Speckle reduction in laser picoprojector by combining optical phase matrix with twin green lasers and oscillating MEMS mirror for coherence suppression," Jpn. J. Appl. Phys. **55**(8S3), 08RF03 (2016).
11. S. Shin, S. Yoo, S. Lee, C. Park, S. Park, J. Kwon, and S. Lee, "Removal of hot spot speckle on laser projection screen using both the running screen and the rotating diffuser," Displays **27**(3), 91–96 (2006).
12. B. Redding, G. Allen, E. Dufresne, and H. Cao, "Low-loss high-speed speckle reduction using a colloidal dispersion," Appl. Opt. **52**(6), 1168–1172 (2013).
13. V. Kumar, K. Usmani, V. Singh, A. Dubey, M. Gupta, and D. Mehta, "Laser speckle reduction using spatially structured and temporally varying beams using double diffractive optical elements," Laser Phys. Lett. **17**(3), 036003 (2020).
14. S. Roelandt, Y. Meuret, G. Craggs, G. Verschaffelt, P. Janssens, and H. Thienpont, "Standardized speckle measurement method matched to human speckle perception in laser projection systems," Opt. Express **20**(8), 8770–8783 (2012).
15. M. Akram, V. Kartashov, and Z. Tong, "Speckle reduction in line-scan laser projectors using binary phase codes," Opt. Lett. **35**(3), 444–446 (2010).
16. W. Thomas and C. Middlebrook, "Non-moving Hadamard matrix diffusers for speckle reduction in laser pico-projectors," J. Mod. Opt. **61**(sup1), S74–S80 (2014).
17. A. Prygun, Y. Morozov, T. Kliuieva, Y. Borodin, and Z. Le, "Completely passive method of speckle reduction utilizing static multimode optical fibre and two-dimensional diffractive optical element," J. Mod. Opt. **66**(16), 1688–1694 (2019).
18. S. Hashimoto, H. Kikuchi, and M. Oka, "Illuminating optical device in image display device and image display device," U.S. patent 7,433,126B2 (7 October 2008).
19. Z. Tong, S. Song, S. Jia, and X. Chen, "Nonsequential speckle reduction method by generating uncorrelated laser Subbeams with equivalent intensity using a reflective spatial light modulator," IEEE Photonics J. **9**(5), 1–8 (2017).
20. Z. Tong, C. Sun, Y. Ma, M. Wang, S. Jia, and X. Chen, "Laser spatial coherence suppression with refractive optical elements toward the improvement of speckle reduction by light pipes," IEEE Access **7**, 172190–172198 (2019).
21. W. Teh, U. Durig, U. Drechsler, C. Smith, and H. Guntherodt, "Effect of low numerical-aperture femtosecond two-photon absorption on (SU-8) resist for ultrahigh-aspect-ratio microstereolithography," J. Appl. Phys. **97**(5), 054907 (2005).
22. A. Mata, A. Fleischman, and S. Roy, "Fabrication of multi-layer SU-8 microstructures," J. Micromech. Microeng. **16**(2), 276–284 (2006).
23. B. Bohl, R. Steger, R. Zengerle, and P. Koltay, "Multi-layer SU-8 lift-off technology for microfluidic devices," J. Micromech. Microeng. **15**(6), 1125–1130 (2005).
24. N. E. Farrington and S. Iezekiel, "Accurate layer thickness control and planarization for multilayer SU-8 structures," J. Micro/Nanolithogr., MEMS, MOEMS **10**(1), 013019 (2011).
25. B. Saleh and M. Teich, *Fundamentals of photonics* (John Wiley & Sons Inc., 2009).